Progress In Electromagnetics Research M, Vol. 95, 105–114, 2020

Design and Analysis of a Stub-Less Capacitive Loaded Branch Line Coupler with Improved Bandwidth Performance

Muquaddar Ali*, Kamalesh K. Sharma, and Rajendra P. Yadav

Abstract—In this paper, a novel branch line coupler with improved bandwidth and reduced size is presented. The size reduction is achieved by means of capacitive loading. The capacitive loaded transmission line implemented in the proposed design eliminates the need of open stubs. The mechanism of size reduction and bandwidth enhancement of the coupler is discussed analytically with the help of its equivalent circuit. A prototype is fabricated and tested to validate the concept. The measured fractional bandwidth is 40%, ranging from 2.8 GHz to 4.2 GHz which is suitable for 5G systems. Moreover, the obtained phase imbalance between the output ports is less than $\pm 5^\circ$ for the entire operating range.

1. INTRODUCTION

A branch line coupler (BLC), also known as quadrature hybrid, splits the input power equally at two output ports with a phase difference of 90°. It is an integral part of wireless communication systems and widely used in antenna beamforming networks, mixers, modulators, amplifiers, etc. [1]. The conventional BLC suffers from limited bandwidth and occupies a large area, because of its geometry. Several size reduction techniques such as meandering of transmission lines [2], space-filling curves [3], slow-wave structure [4], and capacitive loading [5, 6] are exploited earlier to achieve a compact BLC, but these techniques compromise with the bandwidth, and also, the phase imbalance between output ports is not constant in these designs.

A modified version of BLC is presented in [7], in which air-filled coaxial transmission lines with quarter wavelength stubs are used to increase the bandwidth. Though a significant improvement in the bandwidth is achieved, it requires a multilayer structure, and the additional stubs increase its size. Similarly, a planar BLC utilizing quarter-wave impedance transformers and balun structures (closely spaced parallel coupled lines) for bandwidth enhancement are presented in [8] and [9], respectively. These BLCs require additional area for employing impedance transformers and balun structures. Cascaded slow-wave structures are used in [10] to reduce the size of BLC with a simultaneous increase in the bandwidth. Some recent works discussed replacing transmission lines in each branch of the BLC with transmission line loaded with an open stub at the center [11], composite right/left-handed (CRLH) stubs [12], and right-angled triangle artificial transmission lines (ATL) [13]. These CRLH and ATL have higher propagation constant which leads to a compact realization of BLC. Yet the bandwidth of these BLCs remains limited.

For wideband applications, a microstrip patch is investigated as an alternative for the BLC in [14] and further explored in [15] and [16]. The structure of the patch is deformed in [16] with spline-based geometry, for which significant improvement in bandwidth is achieved, but the size remains large. A coupler based on half mode substrate integrated waveguide (SIW) is explored in [17], which achieves a wide bandwidth with a rapidly varying phase difference between output ports. A wideband coupler is reported in [18], which is based on rigid gap waveguide making it bulkier and expensive. A coupler based

Received 27 June 2020, Accepted 23 July 2020, Scheduled 15 August 2020
* Corresponding author: Muquaddar Ali (muquaddar@gmail.com).
The authors are with the Department of Electronics and Communication Engineering, MNIT Jaipur, Rajasthan, India.

on empty substrate integrated waveguide (ESIW) is discussed in [19] which presents a wide bandwidth and stable phase imbalance at the output ports. Although these waveguide based couplers have larger bandwidths than that of a conventional BLC, the footprints of these configurations are very large. Moreover, the phase imbalance between output ports is not constant for most of these configurations, except for patch-based couplers, whose phase imbalance is constant for almost half of the operating frequency range.

In this paper, a novel branch-line coupler with smaller footprint and improved bandwidth is discussed. The size reduction is achieved using a capacitive loading, but unlike conventional techniques, where shunt capacitors are attached to the transmission lines, here, an additional series capacitor is added forming a capacitive π-network, to further increase the capacitance and reduce the overall length of the coupler. Such a capacitive π-network is easy to be implemented by means of a microstrip gap discontinuity without the need of open stubs. Also, it eliminates the need of open stubs required to implement shunt capacitors. The rest of the paper is organized as follows. Section 2 discusses the design principle. In Section 3, the coupler is analysed using second level even-odd mode analysis. The fabrication results are discussed in Section 4.

2. DESIGN PRINCIPLE

Periodic capacitive loading has been widely used for size reduction of branch line couplers (BLC) [5, 6]. The scheme for size reduction using a capacitive π-network is shown in Fig. 1(a). It shows that a simple transmission line is divided into three sections, and a symmetric, reciprocal capacitive π-network is connected across the middle section. The susceptances of shunt and series components of the π-network are jB_1 and jB_2, respectively. Here, the series capacitor with susceptance of jB_2 is added to increase the effective susceptance.

The admittance parameters of π-network and middle transmission line section are given by [1]:

$$Y_\pi = \begin{bmatrix} j(B_1+B_2) & -jB_2 \\ -jB_2 & j(B_1+B_2) \end{bmatrix} \tag{1}$$

$$Y_{tline} = \begin{bmatrix} -j\dfrac{Y}{\tan(\theta_b)} & j\dfrac{Y}{\sin(\theta_b)} \\ j\dfrac{Y}{\sin(\theta_b)} & -j\dfrac{Y}{\tan(\theta_b)} \end{bmatrix} \tag{2}$$

The Y-parameters of the combined middle section can be given by:

$$\begin{aligned} Y &= Y_\pi + Y_{tline} \\ &= \begin{bmatrix} j\left(B_1+B_2-\dfrac{Y}{\tan(\theta_b)}\right) & j\left(\dfrac{Y}{\sin(\theta_b)}-B_2\right) \\ j\left(\dfrac{Y}{\sin(\theta_b)}-B_2\right) & j\left(B_1+B_2-\dfrac{Y}{\tan(\theta_b)}\right) \end{bmatrix} \end{aligned} \tag{3}$$

Corresponding $ABCD$ parameters are as follows

$$\left.\begin{aligned} A &= \frac{Y\cos(\theta_b)-(B_1+B_2)\sin(\theta_b)}{Y-B_2\sin(\theta_b)} \\ B &= j\frac{\sin(\theta_b)}{Y-B_2\sin\theta_b)} \\ C &= j\frac{(Y-B_2\sin(\theta_b))^2-(Y\cos(\theta_b)-(B_1+B_2)\sin(\theta_b))^2}{\sin(\theta_b)(Y-B_2\sin(\theta_b))} \\ D &= \frac{Y\cos(\theta_b)-(B_1+B_2)\sin(\theta_b)}{Y-B_2\sin(\theta_b)} \end{aligned}\right\} \tag{4}$$

It can be approximated to a transmission line of same characteristic admittance and effective length ϕ. The $ABCD$ parameters of such a line are compared with Eq. (4), and ϕ is found to be

$$\phi = \tan^{-1}\left(\frac{\tan(\theta_b)}{1-(B_1+B_2)\tan(\theta_b)/Y}\right) \tag{5}$$

It should be noted that $\phi \geq \theta_b$, if $Y \geq (B_1 + B_2)\tan\theta_b$ and $\theta_b \leq \pi/2$. Therefore, it can be concluded that using such capacitive loading, the effective length of the transmission line section increases significantly. The effective length in the previous work [6], where the series capacitance is not available, is given by

$$\phi' = \tan^{-1}\left(\frac{\tan(\theta_b)}{1 - B_1\tan(\theta_b)/Y}\right) \tag{6}$$

It is clear by the comparison of Eqs. (5) and (6) that $\phi \geq \phi'$. It should be noted that the overall increment in effective length is due to capacitive loading; however, the realization of arbitrary capacitance requires open stubs. So, one of the main objectives of this investigation is to implement a π-network which can be realized without adding extra stubs. It is well known that a capacitive π-network can be implemented by placing a gap discontinuity in the transmission line [1]. Using this concept, two transmission lines of length θ_a and width W are placed in series separated by a distance of W_2. A transmission line of length θ_b is placed across it as shown in Fig. 1(b). For practical implementation, a circularly curved transmission line of length θ_b is placed across this gap, and the effective width at the gap which contributes to the capacitances is W_1. The effect of discontinuities due to the bend structure will be low therefore neglected in the analysis to avoid complexity. The characteristic admittances of all three sections remain the same, and the whole structure approximates in the shape of Greek letter Ω as shown in Fig. 1(c). Thus, a stub-less capacitive loading is achieved using such a structure.

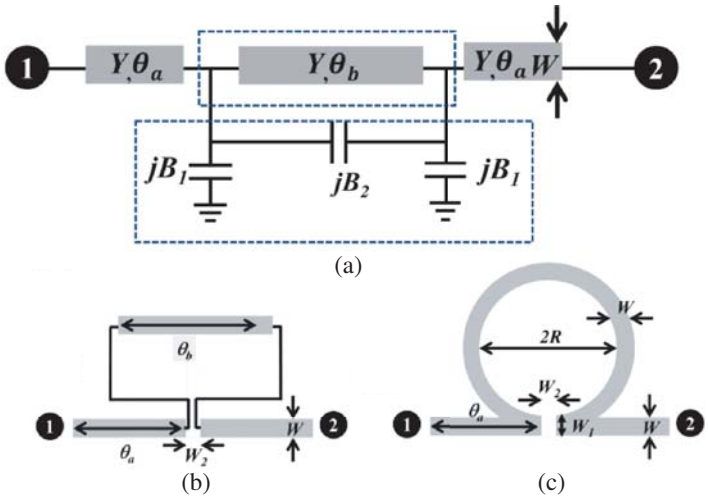

Figure 1. Size reduction scheme (a) transmission line loaded with a capacitive π-network, (b) approximate realization, and (c) practical realized transmission line without any open stub.

3. COUPLER LAYOUT

The schematic diagram of the proposed branch-line coupler consisting of four Ω-shaped transmission line sections is shown in Fig. 2(a). The admittances of horizontal and vertical branches are Y_h and Y_v, respectively. Corresponding design parameters are W_h, W_{h1}, W_{h2}, G_h, W_v, W_{v1}, W_{v2}, G_v, R_h, and R_v. The length and perimeter of the subsections in each branch are L_1 and $2\pi R_{h,v}$.

3.1. Equivalent Circuit Configuration

The working of the presented coupler can be better understood from its equivalent circuit which is shown in Fig. 2(b). As can be seen, it has four branches, consisting of three sub-sections of lengths θ_1, $2\theta_2$, and θ_1, where θ_1 and θ_2 are the electrical lengths corresponding to L_1 and πR, respectively. A symmetric and reciprocal capacitive π-network with shunt and series capacitances of $C_{h1,v1}$ and $C_{h2,v2}$, respectively, is placed as equivalent for the gap discontinuities in each branch. In addition, the entire circuit has two lines of symmetry namely O-O$'$ and Q-Q$'$.

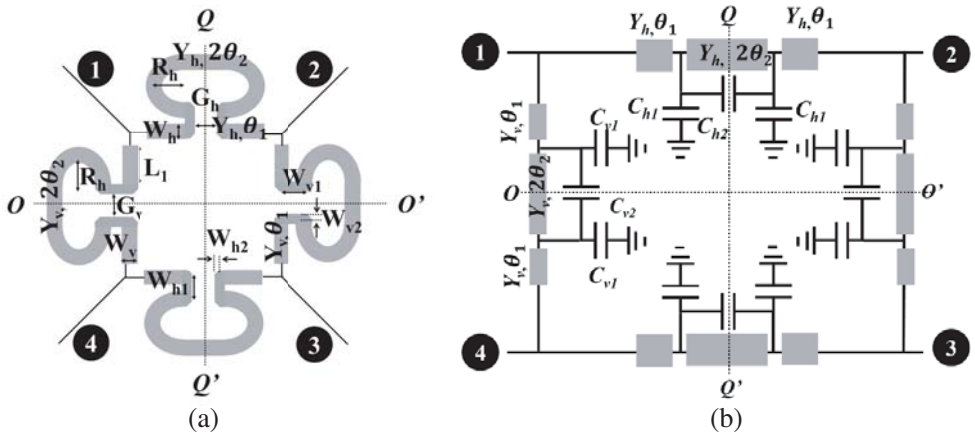

Figure 2. (a) Schematic diagram of proposed branch line coupler, and (b) approximate equivalent circuit.

3.2. Even Odd Mode Analysis

The bisymmetric properties of the circuit allow the use of second order even-odd mode analysis [17]. According to which the performance of above mentioned circuit can be determined by applying superposition theorem in the four combinations of symmetric and antisymmetric excitations, namely even-even, even-odd, odd-even, and odd-odd modes.

The normalized excitation amplitudes at all ports in each case are tabulated in Table 1. The total normalized excitation at port 1 is unity for such combinations. For symmetric and anti-symmetric excitations, either an electric (E) or a magnetic (M) wall can be virtually assigned at the symmetry lines O-O′ and Q-Q′. These boundary conditions in each mode are tabulated in Table 1.

Table 1. Normalized amplitudes and boundary conditions at different lines of symmetry.

Mode	Port#1	Port#2	Port#3	Port#4	B.C. at O-O′	B.C. at Q-Q′
Eveneven	+1/4	+1/4	+1/4	+1/4	H	H
Oddeven	+1/4	+1/4	−1/4	−1/4	E	H
Even-odd	+1/4	−1/4	+1/4	−1/4	H	E
Oddodd	+1/4	−1/4	−1/4	+1/4	E	E

The magnetic boundary condition results in a virtual open circuit whereas the electric boundary acts as a virtual ground. By applying these boundary conditions, quarter circuits are obtained for each mode as shown in Fig. 3. Here, all admittances are normalized to Y_0. In the case of magnetic wall, there is no current passing through the capacitor; therefore, C_{h2} and C_{v2} are considered as open circuits when the magnetic boundary is applied at Q-Q′ and O-O′. On the other hand, in the case of electric wall, a voltage null exists between the capacitor plates; therefore, the effective capacitances are taken as $2C_{h2}$ and $2C_{v2}$. The normalized susceptances offered by C_{h1}, $2C_{h2}$, C_{v1}, and $2C_{v2}$ are denoted by b_{h1}, $2b_{h2}$, b_{v1}, and $2b_{v2}$, respectively.

From the bisymmetry properties, the S-parameters of the structure can be calculated as follows [1]:

$$\left.\begin{aligned} S_{11} = S_{22} = S_{33} = S_{44} &= 1/4(\Gamma_{ee} + \Gamma_{eo} + \Gamma_{oe} + \Gamma_{oo}) \\ S_{21} = S_{12} = S_{34} = S_{43} &= 1/4(\Gamma_{ee} - \Gamma_{eo} + \Gamma_{oe} - \Gamma_{oo}) \\ S_{13} = S_{31} = S_{42} = S_{43} &= 1/4(\Gamma_{ee} - \Gamma_{eo} - \Gamma_{oe} + \Gamma_{oo}) \\ S_{41} = S_{14} = S_{23} = S_{32} &= 1/4(\Gamma_{ee} + \Gamma_{eo} - \Gamma_{oe} - \Gamma_{oo} \end{aligned}\right\} \quad (7)$$

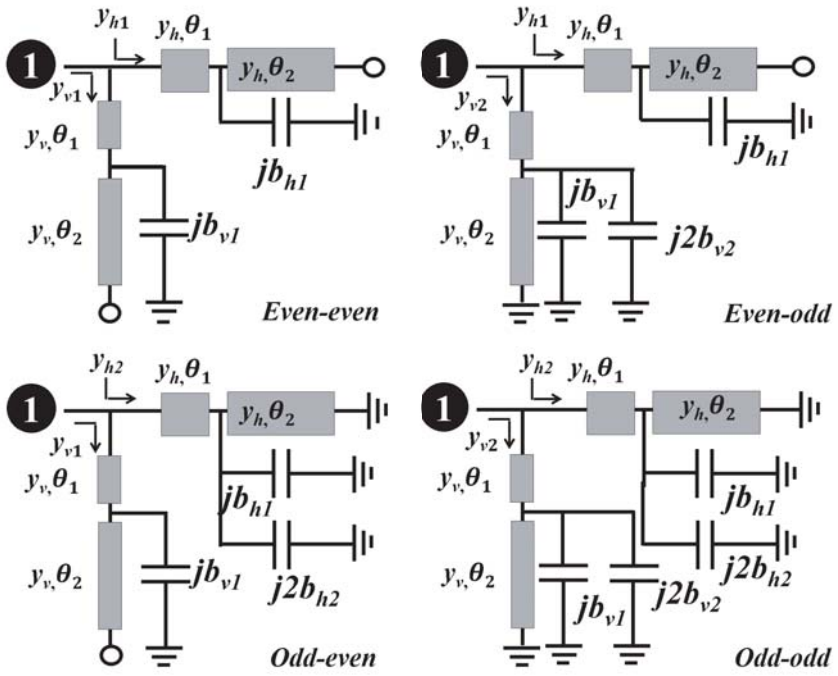

Figure 3. Quarter circuits for second-level even-odd mode analysis.

where Γ_{ee}, Γ_{eo}, Γ_{oe}, and Γ_{oo} are the reflection coefficients in each case and can be calculated by

$$\Gamma_{ab} = (1 - y_{inab})/(1 + y_{inab}),\ for\ a, b = e\ or\ o \tag{8}$$

where,

$$\left.\begin{aligned} y_{inee} &= y_{h1} + y_{v1} \\ y_{inoe} &= y_{h1} + y_{v2} \\ y_{ineo} &= y_{h2} + y_{v1} \\ y_{inoo} &= y_{h2} + y_{v2} \end{aligned}\right\} \tag{9}$$

And

$$\left.\begin{aligned} y_{h1} &= jy_h \frac{y_h(t_1 + t_2) + b_{h1}}{y_h(1 - t_1 t_2) - b_{h1} t_1} \\ y_{h2} &= jy_h \frac{b_{h1} + 2b_{h2} + y_h(t_1 - 1/t_2)}{y_h(1 + t_1/t_2) - (b_{h1} + 2b_{h2}) t_1} \\ y_{v1} &= jy_v \frac{y_v(t_1 + t_2) + b_{v1}}{y_v(1 - t_1 t_2) - b_{v1} t_1} \\ y_{v2} &= jy_v \frac{b_{v1} + 2b_{v2} + y_v(t_1 - 1/t_2)}{y_v(1 + t_1/t_2) - (b_{v1} + 2b_{v2}) t_1} \end{aligned}\right\} \tag{10}$$

3.3. Analytical Results

The impact of various capacitors can be better understood by considering four evolutionary steps or special cases of the final design. Case-I, where all capacitors are open-circuited, as a result the coupler can be equated to a conventional BLC as depicted in Fig. 4(a). Case-II, where $\omega C_{h1} = \omega C_{v1} = b_1$, $\omega C_{h2} = \omega C_{v2} = 0$, $\theta_1 = 0$, and $\theta_2 = \lambda_0/8$. The resultant coupler having four shunt capacitors at each junction is shown in Fig. 4(b), such types of couplers are widely investigated in literature for reduction in the size of couplers [5, 6]. Case-III, where $\omega C_{h1} = \omega C_{v1} = 0$, $\omega C_{h2} = \omega C_{v2} = b_2$, $\theta_1 = 0$, and $\theta_2 = \lambda_0/8$. In this case, a capacitance is connected in parallel to each branch of the coupler as

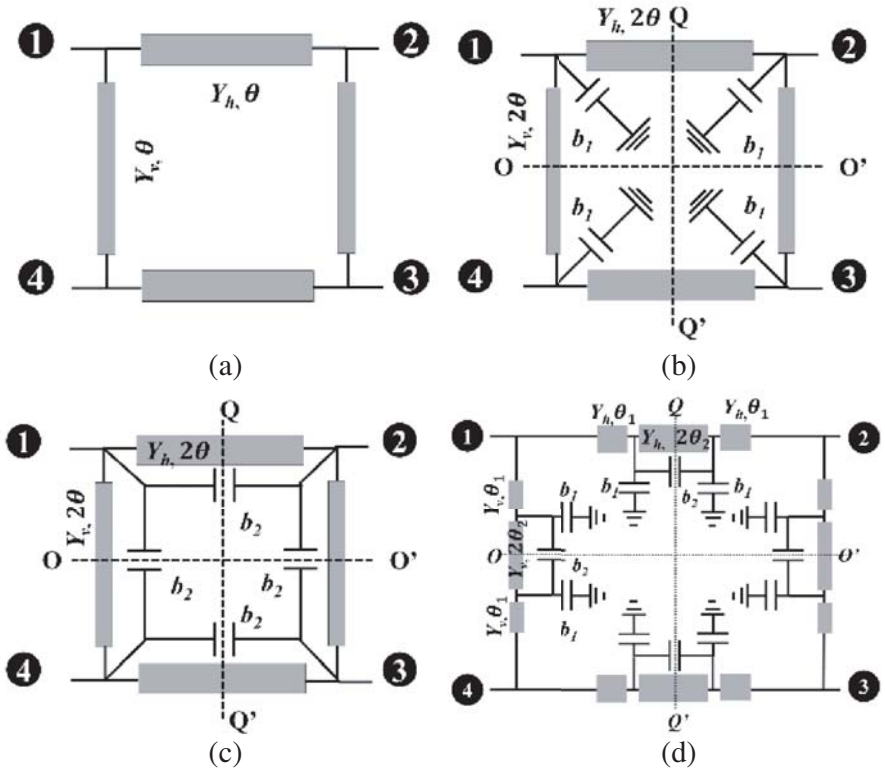

Figure 4. Equivalent circuit in (a) case-I, (b) case-II (c) case-III, and (d) case-IV.

illustrated in Fig. 4(c). Case-IV, where $\omega C_{h1} = \omega C_{v1} = b_1$, $\omega C_{h2} = \omega C_{v2} = b_2$, and $\theta_1 + \theta_2 = \lambda_0/8$. The resulting circuit is shown in Fig. 4(d).

The S-parameters are computed using Equations (6) to (9), for fixed values of y_h, y_v, b_1, b_2 at 1.414, 1, 0.2, and 0.1, respectively. And the length of each branch is kept constant, i.e., $2(\theta_1 + \theta_2) = \lambda_0/4$. The calculated return loss at port 1 and the isolation between ports 1 and 4 are displayed in Fig. 5(a). It can be observed from the figure that the operating frequencies are f_0, $0.9f_0$, $0.95f_0$, $0.85f_0$, and $0.85f_0$ for case-I, case-II, case-III, case-IV with $\theta_1 = 0$ and case-IV with $\theta_1 = \lambda_0/25$, respectively. The operating frequency is reduced by using capacitive loading either in series or shunt, which implies that the electrical size of the coupler gets reduced. Case IV offers the highest equivalent capacitive susceptance, so it provides the most compact size of the coupler. However, the isolation at operating frequency is slightly decreased with an increase in θ_1.

The magnitude imbalance, $\Delta S = S_{31}(\text{dB}) - S_{21}(\text{dB})$, and phase imbalance, $\Delta\theta = \angle S_{31} - \angle S_{21}$, between ports 2 and 3 are shown in Fig. 5(b) for these cases. It is observed that the fractional bandwidths where $\Delta S \leq \pm 1$ dB and $S_{11} \leq -10$ dB, corresponding to these cases are 25%, 33%, 38%, 41%, and 48%, respectively. The proposed design has the highest bandwidth. It should be noted that θ_1 cannot be increased beyond a certain limit, because as θ_1 increases, ΔS becomes more negative, and beyond a certain value it becomes less than -1 dB. The fractional bandwidths for $|\Delta\theta| \leq 2^\circ$ and $S_{11} \leq -10$ dB corresponding to these cases are 25%, 33%, 22%, 25%, and 31%, respectively.

It can also be concluded that in case-II, the size of the coupler is reduced, and its overall performance improves. However, in case-III and case-IV, due to the capacitor placed in parallel to the transmission lines, the fractional bandwidth of magnitude imbalance increases at the cost of increased phase imbalance. It is also obvious from observations that the fractional bandwidth for phase imbalance can be improved by decreasing the length of transmission lines across which parallel capacitor is placed. Thus, optimization of various design parameters such as b_1, b_2, and θ_1 is required to improve the overall performance of the coupler and simultaneously decrease its size.

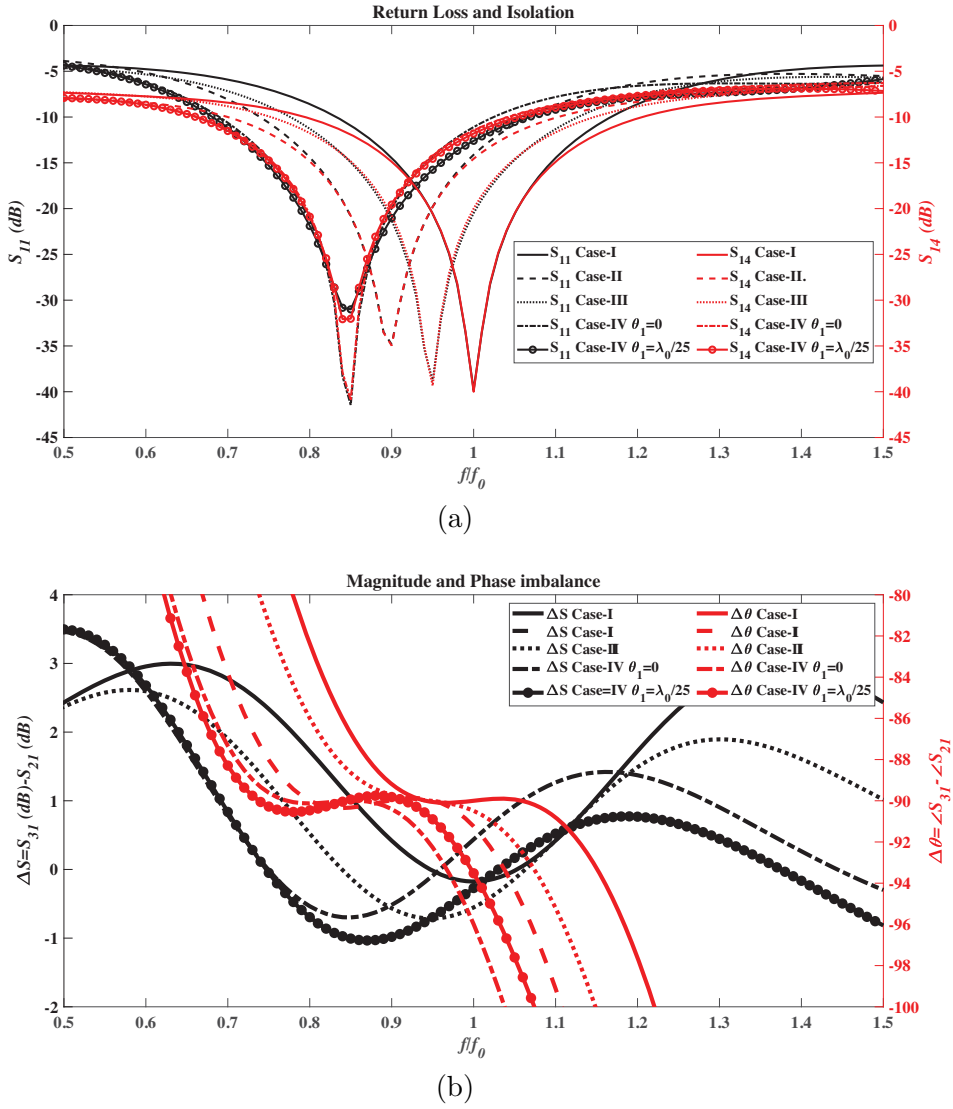

Figure 5. (a) Return loss at port 1 and isolation between port 1 and 4, and (b) magnitude and phase imbalance between ports 2 and 3.

4. FABRICATION AND MEASUREMENT

As discussed earlier, the proposed topology is used because it is most suitable to implement the capacitive loading without the need of additional stubs. To validate the design principle, a BLC is designed to operate at 3.5 GHz, and design dimensions are optimized using Ansys HFSS v17. As capacitors are added in parallel to the horizontal and vertical transmission lines, the effective impedance is decreased; therefore, both impedances are also optimized. The exact capacitive values are difficult to realize, so based upon the discussion in Sections 2 and 3, the design parameters are optimized using EM solver. A multi-objective optimization technique is used to minimize the return loss and isolation S_{11} and S_{41}, respectively, and maximize the bandwidths for magnitude imbalance of $|\Delta S| \leq 1$ dB and phase imbalance $|\Delta\theta| \leq 2^\circ$. The optimum dimensions obtained for horizontal and vertical branches correspond to impedance values of 35 Ω and 63 Ω respectively. For the design RT Duroid 5880 is used as dielectric material with a dielectric constant, loss tangent, and thickness of 2.2, 0.0002, and 0.787 mm, respectively. Microstrip lines of 50 Ω impedance are used for feeding. The optimum design parameters are tabulated below in Table 2.

Table 2. Optimum dimensions of the 90^o branch line coupler

Parameter	Value	Parameter	Value	Parameter	Value	Parameter	Value
W_h	2.9 mm	W_{h1}	1.45 mm	W_{h2}	0.8 mm	R_h	3.8 mm
$W v$	1.7 mm	W_{v1}	1.05 mm	W_{v2}	0.6 mm	R_v	3.8 mm
W_{50}	2.4 mm	L_1	2.45 mm	G_h	0.4 mm	G_v	0.35 mm

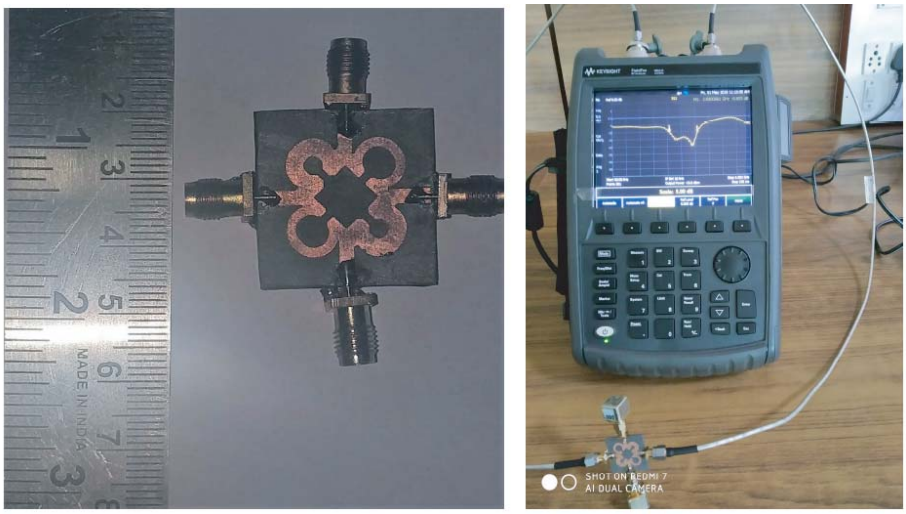

(a) (b)

Figure 6. (a) Photograph of the fabricated prototype, and (b) testing environment while measuring S_{11}.

Table 3. Comparison with recent works.

Ref.	f_0 GHz	Technique	Size $\lambda \times \lambda$	BW ± 1 dB	BW $\delta\theta$
[7]	36.5	Multilayer	0.75×0.75	12.4	-
[9]	2	Balun	1.4×0.68	37.6	45*
[10]	1	Slow Wave	0.28×0.19	32	-
[12]	10	Patch	0.56×0.56	25	3
[13]	10	Patch	0.67×0.78	50	$\leq$15
[14]	10	HMSIW	1.7×1.5	24.6	$\leq$10
[15]	15	RWG	1.6×1.6	14	33
[16]	5	ESIW	0.35×0.65	22	20
This Work	3.5	Stub-less Cap. loading	0.25×0.25	40	40*

A prototype of the designed coupler is fabricated with dimensions given in Table 2. Generic photolithography technique is used for patterning, and ferric chloride is used for etching. The prototype is connected with $50\,\Omega$ transmission lines using SMA connectors. Testing of the coupler is done using Keysight's Field Fox RF Analyzer N9914A. Fig. 6(a) shows a photograph of the prototype, and Fig. 6(b) shows the measurement setup.

The comparison between simulated and measured results is shown in Fig. 7. The measured results are in good agreement with the simulated ones. From Fig. 7(a), it can be observed that equal power

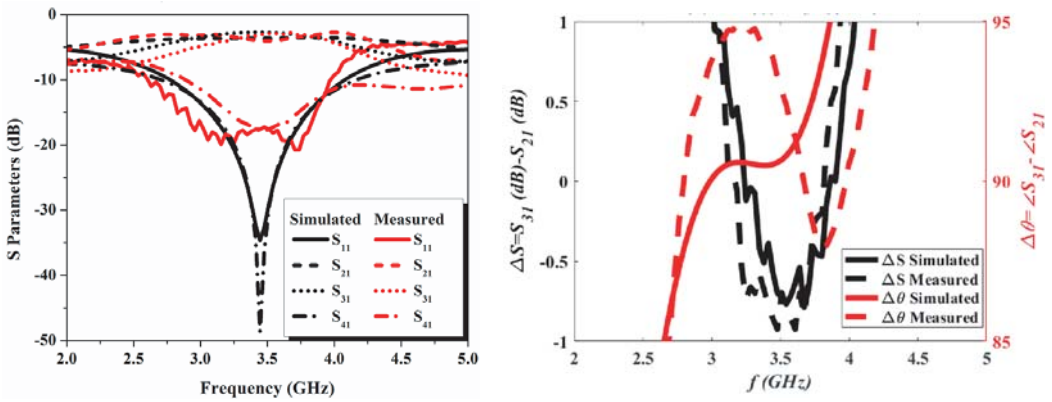

(a) (b)

Figure 7. Comparison of simulated and measured results, (a) S parameters magnitude in dB and (b) phase difference between outputs.

is received at both output ports. A bandwidth of 1.4 GHz, ranging from 2.8 GHz to 4.2 GHz with an amplitude difference of ±1 dB at output ports, is achieved, and the isolation is better than 10 dB in the above range. The phase imbalance between the output ports is displayed in Fig. 7(b). It is observed that the measured phase imbalance for this whole range is ±5°. At the operating frequency (3.5 GHz), the transmission coefficients S_{21} and S_{31} are measured and found to be −3.2 dB and −3.5 dB, respectively, while the return loss and isolation are −18.2 dB and −17.5 dB, respectively.

The performance comparison of the proposed coupler with previously reported structures is tabulated in Table 3. The presented design has much wider bandwidth than other couplers. Also, the phase imbalance between output ports is more stable.

5. CONCLUSION

A compact wideband branch-line coupler using Ω shaped transmission lines is designed, analysed, fabricated, and measured. The concept of implementing a capacitive loaded transmission line without using stubs is discussed and implemented for size reduction of the coupler. The coupler operates from 2.8 GHz to 4.2 GHz, covering the whole range of frequencies designated for 5G applications in sub-6 GHz band. Its footprint is 35% smaller than the conventional BLC, and a broader bandwidth of 40% is achieved. In addition, the phase imbalance between the output ports is less than ±5° for the entire operating range. The smaller footprint and wide bandwidth make it suitable to be integrated with beamforming networks for 5G systems.

ACKNOWLEDGMENT

This work is supported by the Ministry of Electronics & Information and Technology, Govt. of India, under Visvesvaraya PhD Scheme, Grant No. 1000110674.

REFERENCES

1. Pozar, D. M. P., *Microwave Engineering*, 3rd Edition, Wiley, New York, NY, USA, 2005.
2. Kawai, T. and I. Ohta, "Planar-circuit-type 3-dB quadrature hybrids," *IEEE Trans. Microw. Theory Tech.*, Vol. 42, No. 12, 2462–2467, 1994.
3. Ghali, H. and T. Moselhy, "Design of fractal rat-race coupler," *IEEE MTT-S International Microwave Symposium Digest (IEEE Cat. No. 04CH37535)*, Vol. 1, 323–326, Fort Worth, TX, USA, 2004.

4. Wang, J., B. Z. Wang, Y. X. Guo, L. C. Ong, and S. Xiao, "A compact slow-wave microstrip branch-line coupler with high performance," *IEEE Microw. Wirel. Components Lett.*, Vol. 17, No. 7, 501–503, 2007.
5. Eccleston, K. W. and S. H. M. Ong, "Compact planar microstripline branch-line and rat-race couplers," *IEEE Trans. Microw. Theory Tech.*, Vol. 51, No. 10, 2119–2125, 2003.
6. Chun, Y. and J. Hong, "Compact wide-band branch-line hybrids," *IEEE Trans. Microw. Theory Tech.*,, Vol. 54, No. 2, 704–709, Feb. 2006.
7. Wang, Y., M. Ke, M. J. Lancaster, and F. Huang, "Micromachined millimeter-wave rectangular-coaxial branch-line coupler with enhanced bandwidth," *IEEE Trans. Microw. Theory Tech.*, Vol. 57, No. 7, 1655–1660, 2009.
8. Lee, S. and Y. Lee, "Wideband branch-line couplers with single-section quarter-wave transformers for arbitrary coupling levels," *IEEE Microw. Wirel. Components Lett.*, Vol. 22, No. 1, 19–21, 2012.
9. Wu, Y., Q. Liu, S. W. Leung, Y. Liu, and Q. Xue, "A novel planar impedance-transforming tight-coupling coupler and its applications to microstrip baluns," *IEEE Trans. Components, Packag. Manuf. Technol.*, Vol. 4, No. 9, 1480–1488, 2014.
10. Koziel, S. and P. Kurgan, "Design of high-performance hybrid branch-line couplers for wideband and space-limited applications," *IET Microwaves, Antennas Propag.*, Vol. 10, No. 12, 1339–1344, 2016.
11. Kumar, K. V. P. and S. S. Karthikeyan, "Miniaturized quadrature hybrid coupler using modified T-shaped transmission line for widerange harmonic suppression," *IET Microwaves, Antennas Propag.*, Vol. 10, No. 14, 1522–1527, 2016.
12. Wang, C. and W. Tang, "Compact branch-line coupler with harmonic suppression based on a planar simplified dual composite right/left-handed transmission line structure," *Progress In Electromagnetics Research M*, Vol. 69, 127–138, 2018.
13. Geng, L., G.-M. Wang, B.-F. Zong, M.-K. Hu, and H.-Y. Zeng, "Miniaturized branch-line coupler with wide upper stopband using right-angled triangle artificial transmission line," *Progress In Electromagnetics Research Letters*, Vol. 88, 137–142, 2020.
14. Chan, K. L., P. A. Alhargan, and S. R. Judah, "A quadrature-hybrid design using a four-port elliptic patch," *IEEE Trans. Microw. Theory Tech.*, Vol. 45, No. 2, 307–310, 1997.
15. Zheng, S. Y., J. H. Deng, Y. M. Pan, and W. S. Chan, "Circular sector patch hybrid coupler with an arbitrary coupling coefficient and phase difference," *IEEE Trans. Microw. Theory Tech.*, Vol. 61, No. 5, 1781–1792, 2013.
16. Bekasiewicz, A. and S. Koziel, "Novel structure and design of enhanced-bandwidth hybrid quadrature patch coupler," *Microw. Opt. Technol. Lett.*, Vol. 60, No. 12, 3073–3076, 2018.
17. Zou, X., C. M. Tong, C. Z. Li, and W. J. Pang, "Wideband hybrid ring coupler based on half-mode substrate integrated waveguide," *IEEE Microw. Wirel. Components Lett.*, Vol. 24, No. 9, 596–598, 2014.
18. Shams, S. I. and A. A. Kishk, "Design of 3-dB hybrid coupler based on RGW technology," *IEEE Trans. Microw. Theory Tech.*, Vol. 65, No. 10, 3849–3855, 2017.
19. Merello, J. M., V. Nova, C. Bachiller, J. R. Sanchez, A. Belenguer, and V. E. B. Esbert, "Miniaturization of power divider and 90° hybrid directional coupler for C-band applications using empty substrate-integrated coaxial lines," *IEEE Trans. Microw. Theory Tech.*, Vol. 66, No. 6, 3055–3062, 2018.
20. Wang, Y., A. M. Abbosh, and B. Henin, "Broadband microwave crossover using combination of ring resonator and circular microstrip patch," *IEEE Trans. Components, Packag. Manuf. Technol.*, Vol. 3, No. 10, 1771–1777, 2013.
21. Liu, S. and F. Xu, "Minimized multi-layer substrate integrated waveguide 3-dB small aperture coupler," *Microw. Opt. Technol. Lett.*, Vol. 59, 3201–3205, 2017.
22. Manoochehri, O., A. Darvazehban, and D. Erricolo, "UWB double-ridge waveguide coupler with low loss," *Microw. Opt. Technol. Lett.*, Vol. 59, 1787–1791, 2017.